Monthly Notices of the ROYAL ASTRONOMICAL SOCIETY

MNRAS **470,** L64–L68 (2017) doi:10.1093/mnrasl/slx077
Advance Access publication 2017 May 23

CO excitation in the Seyfert galaxy NGC 7130

F. Pozzi,[1,2]★ L. Vallini,[3] C. Vignali,[1,2] M. Talia,[1] C. Gruppioni,[2] M. Mingozzi,[1,4] M. Massardi[5] and P. Andreani[6]

[1]*Dipartimento di Fisica e Astronomia, Università degli Studi di Bologna, Via Berti Pichat 6/2, I-40127 Bologna, Italy*
[2]*INAF – Osservatorio Astronomico di Bologna, Via Ranzani 1, I-40127 Bologna, Italy*
[3]*Nordita, KTH Royal Institute of Technology and Stockholm University, Roslagstullsbacken 23, SE-106 91 Stockholm, Sweden*
[4]*INAF – Osservatorio Astrofisico di Arcetri, largo E. Fermi 5, I-50127 Firenze, Italy*
[5]*INAF – Osservatorio di Radioastronomia, Via Piero Gobetti 101, I-40129 Bologna, Italy*
[6]*European Southern Observatory, Karl-Schwarzschild-Strasse 2, D-85748 Garching, Germany*

Accepted 2017 May 11. Received 2017 May 9; in original form 2017 February 21

ABSTRACT

We present a coherent multiband modelling of the carbon monoxide (CO) spectral energy distribution of the local Seyfert galaxy NGC 7130 to assess the impact of the active galactic nucleus (AGN) activity on the molecular gas. We take advantage of all the available data from X-ray to the submillimetre, including ALMA data. The high-resolution (∼0.2 arcsec) ALMA CO(6–5) data constrain the spatial extension of the CO emission down to an ∼70 pc scale. From the analysis of the archival *Chandra* and *NuSTAR* data, we infer the presence of a buried, Compton-thick AGN of moderate luminosity, $L_{2-10\,\mathrm{keV}} \sim 1.6 \times 10^{43}$ erg s^{-1}. We explore photodissociation and X-ray-dominated-region (PDR and XDR) models to reproduce the CO emission. We find that PDRs can reproduce the CO lines up to $J \sim 6$; however, the higher rotational ladder requires the presence of a separate source of excitation. We consider X-ray heating by the AGNs as a source of excitation, and find that it can reproduce the observed CO spectral energy distribution. By adopting a composite PDR+XDR model, we derive molecular cloud properties. Our study clearly indicates the capabilities offered by the current generation of instruments to shed light on the properties of nearby galaxies by adopting state-of-the-art physical modelling.

Key words: photodissociation region (PDR) – galaxies: active – galaxies: ISM.

1 INTRODUCTION

In the far-infrared (FIR) and submillimetre range, there are several molecular and atomic lines that probe the different phases of the interstellar medium (ISM) and whose study gives important constraints on its physical condition. In particular, the carbon monoxide (CO) molecule is a good tracer of the molecular gas phase, being the second most abundant molecule after the molecular hydrogen (H_2).

The CO spectral line energy distribution (i.e. CO SLED) is sensitive to the molecular gas kinetic temperature and can provide constraints on the dominant heating mechanism, controlled by radiative heating from stars and active galactic nuclei (e.g. AGNs; Obreschkow et al. 2009). While the CO SLED line fluxes usually rise up to the CO(5–4) transition and then decrease for a typical region around newly formed stars ('photondissociated region', PDR), the high rotational transition levels, if excited, trace the presence of warm gas ($100 < T < 1000$ K) heated by X-ray photons ('X-ray-dominated regions', XDRs; e.g. van der Werf et al. 2010) or by shocks (e.g. Panuzzo et al. 2010; Meijerink et al. 2013). This has been shown first with observations from ground-based telescopes, mainly for high-z galaxies and AGNs, taking advantage of the possibility to probe the rest-frame mid-/high-J transitions ($\nu > 500$–600 GHz) with submillimetre/millimetre facilities such as the IRAM and CARMA interferometers (i.e. Solomon & Vanden Bout 2005). Subsequently, the *Herschel* satellite has extended the CO detections to high transitions levels also in the local Universe, using both the PACS and SPIRE/FTS spectrometers (Pereira-Santaella et al. 2013; Rosenberg et al. 2015). With the advent of the submillimetre/millimetre ALMA telescope, a further step has been taken in this field, thanks to its high instantaneous sensitivity and spatial resolution. In the local Universe, regions of the order of 50–100 pc can be easily resolved, supplying crucial information on the modelling.

NGC 7130 is a local ($z = 0.0161$) luminous IR galaxy ($L_{\mathrm{IR}} \sim 10^{11.3}$ L$_\odot$; see Gruppioni et al. 2016) with an 'ambiguous' nature. On the one hand, it was optically morphologically classified as a peculiar Sa spiral galaxy (Lu 1998) and, on the other hand, as a Seyfert 1.9 source from the optical emission-line ratio (Véron-Cetty

★ E-mail: f.pozzi@unibo.it

& Véron 2006). Recently, from a spectral energy distribution (SED) decomposition analysis, Gruppioni et al. (2016) found that the data were well reproduced without the need of an AGN torus component. On the other hand, the presence of a buried or low-luminosity AGN is suggested by the fine-structure IR lines and X-ray data. In the mid-IR, Tommasin et al. (2010) detected [Ne V] lines at 14.32 and 24.31 μm, which, due to their high ionization potential of 97 eV, can be reasonably excited only by an AGN. In the far-IR, Spinoglio et al. (2015) found a low [O III]88 μm/[O IV]26 μm ratio (∼1), similar to other Seyfert rather than to starburst galaxies. In the X-ray band, Levenson et al. (2005), analysing *Chandra* data, claimed the presence of a buried Compton-thick AGN ($N_{\rm H} > 10^{24}$ cm^{-2}) with observed low luminosity ($L_{0.5-10} \sim 10^{41}$ erg s^{-1}), dominating at energies > 2 keV. From the Kα iron emission line, the same authors estimated an intrinsic 2–10 keV luminosity of $\sim 10^{43}$ erg s^{-1}. Indications of extreme obscuration towards this source came also from Risaliti, Maiolino & Salvati (1999) on the basis of the 2–10 keV/[O III] flux ratio. Summarizing, NGC 7130 seems to be a prototype of a strong starburst probably hosting a Compton-thick AGN.

The goal of this Letter is to definitively assess the impact of the AGN activity on the molecular gas in NGC 7130. This will be achieved via the modelling of the NGC 7130 CO SLED. A coherent multiphase (and multiband) analysis of NGC 7130 build upon literature data and new X-ray observations will be presented. The Letter is structured as follows: In Section 2, we provide details on the new *Chandra* and *NuSTAR* data, and we highlight the importance of the high-resolution ALMA archival observations in devising a precise CO SLED model. In Section 3, we present the model assumptions and the results. Finally, in Section 4, we draw a short summary.

2 DATA

2.1 *Chandra* and *NuSTAR* data

NGC 7130 was observed by *Chandra* in Cycle 2 with the ACIS-S3 CCD at the aimpoint (on 2001 October 23), for an exposure time of 38.6 ks. The source shows a point-like emission surrounded by diffuse emission, as extensively described by Levenson et al. (2005). We extracted the *Chandra* spectrum using a circular region of 15-arcsec radius (to include the nuclear and the diffuse emission, and have enough photon statistics for a proper spectral modelling), and the background from a circular region (radius of 22 arcsec) with no sign of diffuse emission. The spectrum, of about ≈3600 net counts, was rebinned to have at least 25 counts per bin to apply χ^2 statistics within the XSPEC package (Arnaud 1996).

NuSTAR observed NGC 7130 on 2014 August 17 for an exposure time of 21.2 ks. Data were reprocessed and screened using standard settings and the NUPIPELINE task, and source and background spectra (plus the corresponding response matrices) were extracted using NUPRODUCTS. Given the relatively low flux of the source, a circular extraction region of 30″arcsec radius was selected, while a background was extracted from two nearby circular regions of 40-arcsec radius. The source net counts, ≈190 and ≈220 in the FPMA and FPMB cameras, respectively, were rebinned to 20 counts per bin. The source signal is detected up to ≈30 keV.

Chandra and *NuSTAR* data were fitted simultaneously with the same modelling, which accounts for the dominant thermal emission in the soft X-rays (*Chandra* band) and for the nuclear emission at hard X-ray energies (*NuSTAR* range), see Fig. 1. In particular, data below a few keV are modelled with two thermal components (MEKAL model within XSPEC), similarly to Levenson et al. (2005). The derived

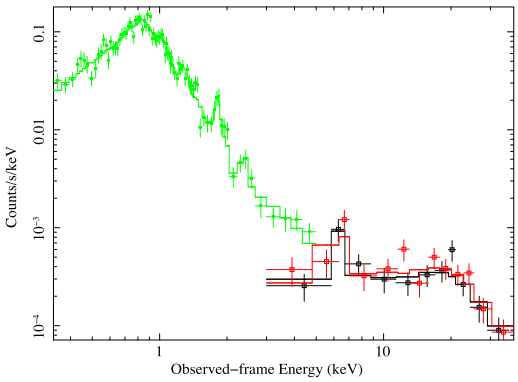

Figure 1. *Chandra* (green points) and *NuSTAR* FPMA and FPMB (black and red points, respectively) spectra of NGC 7130 and best-fitting modelling (see the text for details).

plasma temperatures are $kT_1 = 0.59^{+0.04}_{-0.05}$ and $kT_2 = 1.58^{+0.93}_{-0.37}$ keV. Four additional lines, likely related to iron and Si XIII transitions, seem to be required (at a statistical level of at least 90 per cent). The *Chandra* data appear very noisy above ≈5 keV and were therefore removed; however, in this energy range, *NuSTAR* data, albeit characterized by a lower spectral resolution (≈400 versus 130 eV typically provided by *Chandra* at 6 keV), are fundamental to characterize the iron K α emission line, to define the intrinsic continuum of NGC 7130 and to place constraints on the level of obscuration. To achieve these goals, we used the MYTORUS model (Murphy & Yaqoob 2009), which is based on Monte Carlo simulations and, assuming a toroidal geometry for the reprocessor (uniform and cold), self-consistently includes reflection and scattering. While the photon index was fixed to 1.9, as typically observed in AGNs and quasars, the column density of the torus and the inclination angle between the observer's line of sight and the symmetry axis of the torus $\theta_{\rm obs}$ are left as free parameters of the fit. We obtain an equatorial column density of $(5.3 \pm 1.6) \times 10^{24}$ cm^{-2} and $\theta_{\rm obs} = 79^\circ \pm 5^\circ$. This overall modelling provides a χ^2/dof (degrees of freedom) of 99.1/85; most of the deviations from the best-fitting model appear in the soft band and are of limited relevance for the purposes of the present X-ray analysis. The intrinsic 2–10 and 1–100 keV luminosities of the AGNs are 1.6×10^{43} and 5.1×10^{43} erg s^{-1}, respectively.

Our results are in good agreement with the analysis of the hard-X-ray data (*NuSTAR* and *Swift*/BAT) from Koss et al. (2016), where NGC 7130 was defined as a moderate Compton-Thick AGN, and with the recent work of Ricci et al. (2017), who are performing an analysis similar to ours, confirming the presence of CT obscuration.

2.2 CO data

The observed CO SLED is shown in Fig. 2. The mid-/high-*J* levels ($J_{\rm up} > 4$) are from *Herschel* SPIRE/FTS observations (Pereira-Santaella et al. 2013), while the low-*J* transitions are from Albrecht, Krügel & Chini (2007) using the Swedish ESO Submillimeter Telescope (SEST). The *Herschel* observations are performed to cover a field of view (FOV) of ∼2 arcmin. The observations performed with the single-dish SEST telescope are pointed observations with an FOV (∼2 × FWHM, where FWHM is full width at half-maximum) of ∼1 arcmin. NGC 7130 appears point-like (Pereira-Santaella et al. 2013) in the *Herschel* SPIRE photometric bands (from 250 to 500 μm) characterized by a maximum FWHM of 40 arcsec. Assuming that the dust (sampled by the SPIRE photometric observations)

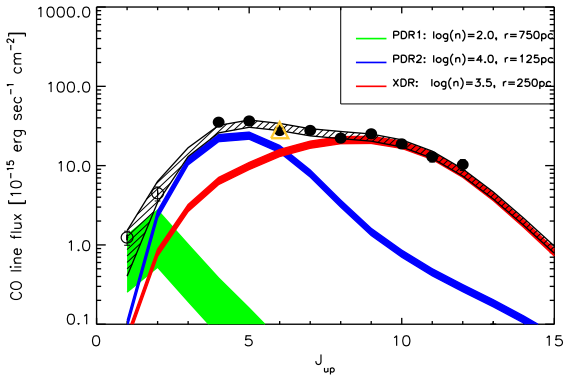

Figure 2. Observed CO SLED and best-fitting model overplotted. The low-J transitions (open circles) are from the SEST telescope, while the mid-/high-J transition levels (filled circles) are from *Herschel* SPIRE/FTS observations. The CO(6–5) ALMA data are highlighted as a yellow triangle. The green, blue and red lines correspond to the three model components (parameters reported in the legend). The black line is the sum of the three components. The thickness of the coloured regions represents the 1σ uncertainties.

and the gas (sampled by SPIRE/FTS observations) are almost co-spatial, this means that all the CO fluxes correspond to the integrated emission of the galaxy.

The yellow triangle represents the new ALMA CO(6–5) data from Zhao et al. (2016). For details on the analysis of the ALMA data, refer to Zhao et al. (2016); here, we remind only the points that are relevant for our analysis. The ALMA observations have been performed in Cycle 2 (project 2013.1.00524.S, PI: Nanyao Lu) with the Band 9 receiver searching for the CO(6–5) transition at 691.473 GHz. The configuration user (C34-5) allowed a synthesized beam FWHM of $\sim 0.20 \times 0.14$ arcsec^2 corresponding to physical scales of $\sim 70 \times 49$ pc^2. The total line flux is 1230 ± 74 Jy km s^{-1}, and half of this flux is contained in a nuclear region of diameter $\sim$500 pc, while the rest is contained in structures at distances of $\sim$500 pc from the centre. The ALMA flux is completely consistent with the *Herschel* measurement (see also Lu et al. 2017). This suggests that the ALMA observation has collected all the CO(6–5) flux, despite that the largest angular scales recovered by the ALMA configuration are only $\sim$3 arcsec, corresponding to $\sim$1 kpc.

3 ISM MODELLING

We model the CO SLED using the version c13.03 of the photoionization/photodissociation code CLOUDY (Ferland et al. 2013), in order to infer the conditions of the molecular gas where the different CO transition lines are excited. In this work, we run two sets of CLOUDY models that assume the molecular clouds to be a 1D gas slab with constant density located at a fixed distance d from the source of the illuminating radiation (e.g. Vallini et al. 2017). We adopt different prescriptions for the SED of the impinging radiation field. The first set of runs (PDR models) assumes a pure stellar SED illuminating the gas slab. The SED is obtained with the stellar population synthesis code STARBURST99 (Leitherer et al. 1999), assuming a Salpeter (Salpeter 1955) initial mass function in the range 1–100 M$_\odot$, and Lejeune–Schmutz stellar atmospheres (Schmutz, Leitherer & Gruenwald 1992; Lejeune, Cuisinier & Buser 1997). We adopt $Z_* = Z_\odot$, and a continuous star formation normalized to reproduce NGC 7130 of SFR $\sim$ 21 M$_\odot$ yr^{-1} (Gruppioni et al. 2016). The second set of runs (XDR models) follows the same approach as proposed by Abel & Satyapal (2008) for modelling the AGN radiation impinging a gas slab. More precisely, to account for the radiation field from the AGNs, we adopt the `table AGN` command in CLOUDY (Korista, Ferland & Baldwin 1997). This command simulates an ultraviolet (UV) bump [$f \propto \nu^{-0.5}\exp(-h\nu/kT_{\rm cut})$] plus an X-ray power law (ν^{-1}). For the value of $T_{\rm cut}$, we use the value 10^6 K proposed by Korista et al. (1997) and adopted in Abel & Satyapal (2008). The ratio of the UV and X-ray continua ($a_{\rm OX}$) is fixed to -1.4, a typical value for an AGN (Zamorani et al. 1981). We normalize the spectrum to match the observed $L_{1-100\,\rm keV} \sim 5 \times 10^{43}$ erg s^{-1} (see Section 2.1).

For the PDR models, we run a total of 35 CLOUDY simulations leaving (i) the gas density n, and (ii) the distance d between the radiation source and the cloud free to vary in the range $\log(n/{\rm cm}^{-3}) = [2\text{–}4.5]$ and $d = [75\text{–}250]$ pc, respectively. Note that a variation in d translates into different values for the impinging far-UV flux (FUV 6–13.6 eV, for the PDR models), and X-ray 1–100 keV flux ($f_{\rm X}$, for XDR models) at the cloud surface. The incident FUV flux (X-ray flux) is a key parameter influencing the heating and cooling processes in the photodissociation (X-ray-dominated) regions (e.g. Hollenbach & Tielens 1999; Meijerink, Spaans & Israel 2007). The former is usually normalized to the solar neighbourhood value (1.6×10^{-3} erg s^{-1} cm^{-2}; Habing 1968) and is indicated with G_0. The chosen density range allows us to sample the typical densities observed in giant molecular clouds (GMCs; e.g. McKee & Ostriker 2007, and references therein). To constrain the parameter d, we take advantage of the key information provided by the ALMA observations. As a matter of fact, d can range from the minimum spatial scale recovered by ALMA ($\sim$70 pc; see Section 2.2) to the maximum extension of the ALMA CO(6–5) detection (radius $\sim$250 pc; see Section 2.2). We also simulate two distances larger than the CO(6–5) emission ($d = [500,750]$ pc). Indeed, the constraint relative to the extension of the CO emission [concerning CO(6–5), and likely also the higher and denser J-transitions] is not applicable to the lower and more diffuse transitions, given the spatial resolution of the *Herschel* and SEST observations (see Section 2.2). For the XDR models, we keep the same range for d as adopted for the PDR models (up to $d = 250$ pc), while we consider a slightly higher density range, i.e. $\log(n/{\rm cm}^{-3}) = [3.5\text{–}5.5]$. With our choice of d, we cover the range $G_0 = (4.9\text{–}410) \times 10^2$ and $f_{\rm X} = 0.3\text{–}80$ in erg s^{-1} cm^{-2}.

For both the PDR and XDR models, CLOUDY computes the emergent CO line emissivity ($\epsilon_{{\rm CO},J-J-1}$, with J varying from 1 to 11) as a function of the depth the radiation penetrates into the cloud. In our models, we set a maximum total gas column density $\log(N_{\rm H}/{\rm cm}^{-2}) = 23$.

In Fig. 3, we show the CO(5–4)/CO(4–3) (top panel) and the CO(10–9)/CO(5–4) (bottom panel) ratios as a function of n and $N_{\rm H}$, obtained with a set of PDR models fixed at $d = 250$ pc, from the stellar radiation source. This spatial scale is equal to the extension of the CO(6–5) emission observed with ALMA by Zhao et al. (2016). The simultaneous study of the two ratios is essential to understand whether the CO SLED can be reproduced by a unique set of PDR models with clouds at fixed distance d from the galaxy centre, or additional components are needed. In Fig. 3 (top panel), the white line highlights the parameter space in n and $N_{\rm H}$, which can reproduce the observed CO(5–4)/CO(4–3)) ratio. These parameter ranges, typical of PDRs, do not reproduce the observed CO(10–9)/CO(5–4) ratio. Hence, for reproducing the mid- to high-J CO transition, there are two possibilities: (1) a PDR + a component that accounts for the contribution of the shock-heated gas, and (2) a PDR + an XDR. We favour the scenario (1) (PDR+XDR), as the most likely one, on the basis of the following considerations.

A chemistry driven by shocks (scenario 2; supported by Pereira-Santaella et al. 2014) is unlikely, given the observed $L_{\rm CO}/L_{\rm IR}$ ratio.

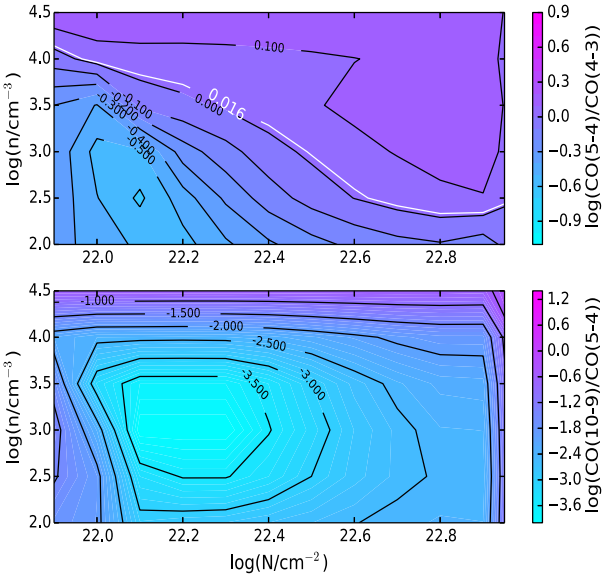

Figure 3. CO(5–4)/CO(4–3) (top panel) and CO(10–9)/CO(5–4) (bottom panel) ratios as a function of the density n and column density $N_{\rm H}$ for PDRs. The distance is fixed ($d = 250$ pc). The white line (top panel) highlights the parameter space corresponding to the observed ratio [log(CO(5–4)/CO(4–3)) = 0.017]. The observed log(CO(10–9)/CO(5–4)) ratio of −0.29 is not reproduced (bottom panel).

As reported in Gallerani et al. (2014), a key difference between shocks and radiative excitation by UV and/or X-rays is that shocks do not heat dust as effectively as they do for gas. NGC 7130 has an observed $L_{\rm CO}/L_{\rm FIR}$ ratio $\sim 1.5 \times 10^{-4}$, a factor typical of XDR/PDR models (e.g. Meijerink & Spaans 2005), while a value of $\sim 7 \times 10^{-4}$, as found by Meijerink et al. (2013) in NGC 6240, seems to be more related to shocks, compressing the gas and heating it to higher temperatures, while not affecting the dust (see also Lee et al. 2016). Moreover, X-ray photons, as the primary heating mechanism of the high-J CO lines, are supported by the following: (i) the clear detection, thanks mostly to *NuSTAR* data, of a hard X-ray flux originating from a central accreting engine (see Section 2.1); and (ii) by the presence of mid-IR [Ne v], which is a clear sign (Tommasin et al. 2010; Gruppioni et al. 2016) of the effect of AGN activity on the ISM of the host galaxy.

Given the considerations reported above, we consider three components: a PDR and one XDR for the mid- to high-J CO transitions, embedded in a more rarefied and extended PDR envelope accounting for the low-J transition. A similar model was presented by van der Werf et al. (2010) for reproducing the CO SLED of Mrk 231. In Fig. 2, our best-fitting model is presented. We find the best fit by a χ^2-minimization routine with nine free parameters: the density, the radiation field intensity and the normalization for each of the three components. We fix the column density $N_{\rm H} \sim 10^{22}$ cm^{-2} for the PDRs and $N_{\rm H} \sim 10^{23}$ cm^{-2} for XDRs. As shown by Meijerink & Spaans (2005, see also McKee & Ostriker 2007; Cormier et al. 2014), while in PDRs the CO-to-atomic carbon ratio (CO/C) ratio rises by 4 dex from the illuminated cloud surface to $N_{\rm H} \sim 10^{22}$ cm^{-2}, in XDRs, CO/C remains almost constant up to $N_{\rm H} \sim 10^{22}$ cm^{-2} and then increases slowly.

The 1σ level of confidence on the normalizations reported in Fig. 2 has been obtained by marginalizing over the other parameters and considering a $\Delta\chi^2 = 3.5$ (see Lampton, Margon & Bowyer 1976). According to our model, the PDR and XDR reproducing the mid-J and high-J transitions are characterized by gas density $\log(n/{\rm cm}^{-3}) = 4.0$ (3.5), and the gas is located at 125 pc (250 pc) from the source of radiation, respectively (corresponding to $G_0 = 4.4 \times 10^3$ and $f_{\rm X} = 5.3$ erg cm^{-2}s^{-1}). The typical thickness and gas temperature of the CO-emitting regions for the PDR and XDR are $l \sim 0.3$, 4 pc and $T = 40$, 100 K, respectively. As expected, X-ray photons keep the gas temperature higher at larger depths. The diffuse PDR component, accounting for the low-J lines, is characterized by a low-density gas [$\log(n/{\rm cm}^{-3}) = 2$] exposed to an FUV flux $G_0 = 4.9 \times 10^2$. The emission originates from regions of thickness $l = 20$ pc, typical of the GMC in the MW (see Murray 2011). The gas temperature is $T = 25$ K.

The presence of, at least, two temperature components to model the CO SLED of NGC 7130 is consistent with the results found in star-forming galaxies (i.e. Daddi et al. 2015; Kamenetzky et al. 2016). The presence of an extra XDR component extends to lower X-ray luminosities (by a factor of ∼4), the result found by van der Werf et al. (2010) for modelling the high-J levels of the local CT-AGN Mrk 231.

The total cold gas mass necessary to fit the CO observation is $M_{\rm cold} \sim 10^9$ M$_\odot$ and completely dominating the total mass. Considering the observed CO(1–0) luminosity ($L_{\rm CO} = 10^{8.8}$ pc^2 K km s^{-1}), the estimated gas mass allows us to directly estimate the CO-to-H$_2$ conversion factor, $\alpha_{\rm CO} = 1.1$ M$_\odot$ pc^{-2} K km s^{-1} (where $M_{\rm cold} = \alpha_{\rm CO} L_{\rm CO}$; see Solomon & Vanden Bout 2005). The CO-to-H$_2$ conversion factor shows a wide range of values reflecting the different ISM conditions (see fig. 12 from the review of Bolatto, Wolfire & Leroy 2013). The normal galaxy discs return high values for $\alpha_{\rm CO}$ ($\alpha_{\rm CO} = 4.6$ M$_\odot$ pc^{-2} K km s^{-1} for the MW; Solomon & Barrett 1991), while $\alpha_{\rm CO}$ drops to very low values (up to $\alpha_{\rm CO} = 0.3$ M$_\odot$ pc^{-2} K km s^{-1}) for active and ultraluminous IR galaxies (see also Downes & Solomon 1998; Papadopoulos et al. 2012). The value found is consistent with the overall properties of NGC 7130 being an LIRG galaxy hosting a moderate, obscured AGN.

4 SUMMARY

In this Letter, we have presented a detailed modelling of the molecular gas in NGC 7130 through the study of the CO SLED. Key information is derived from the ALMA data of the CO(6–5) transition and from the X-ray *Chandra* + *NuSTAR* data. The high-resolution ALMA data allow us to constrain the physical CO emission down to ∼70 pc scales, while the X-ray data confirm the presence of a central highly obscured AGN.

According to our modelling, three components are needed to reproduce the CO SLED: a PDR with parameters typical of the diffuse cold ISM ($\log(n/{\rm cm}^{-3}) = 2.0$, $T \sim 25$ K); a PDR, at relatively higher density and temperatures ($\log(n/{\rm cm}^{-3}) = 4.0$, $T \sim 40$ K); and an extra warm XDR component for $\log(n/{\rm cm}^{-3}) = 3.5$, $T \sim 100$ K. An XDR-driven chemistry for the high-J CO lines is supported by our multicomponent χ^2-fitting the CO SLED. The presence of an XDR is discussed against heating due to shocks. Our modelling predicts a cold gas mass of $M_{\rm cold} \sim 10^9$ M$_\odot$, which implies a CO-to-H$_2$ conversion factor $\alpha_{\rm CO} = 1.1$ M$_\odot$ pc^{-2} K km s^{-1}.

These results show the strength of combining multiband and multiresolution data to assess the impact of the AGNs and star formation activity on the physics of molecular gas. The future exploitation of the data in the ALMA archive will allow us to enlarge the sample and place the results on NGC 7130 in a more statistically significant context. Moreover, we intend to extend the analysis performed on the CO to other molecules, such as HCN and HCO$^+$. These molecules, characterized by high critical densities ($\log(n/{\rm cm}^{-3})$

$\gtrsim 5$), allow us to trace different parameter spaces of the GMCs, and their flux ratios permit us to highlight the presence and strength of an AGN (i.e. Imanishi, Nakanishi & Izumi 2016).

ACKNOWLEDGEMENTS

We acknowledge support from the Italian node of the Alma Regional Center. This Letter makes use of the ALMA data ADS/JAO.ALMA#2013.1.00524.S. FP kindly thanks the referees Matthew Malkan and Andrea Cimatti.

REFERENCES

Abel N. P., Satyapal S., 2008, ApJ, 678, 686
Albrecht M., Krügel E., Chini R., 2007, A&A, 462, 575
Arnaud K. A., 1996, in George H. J., Jeannette B., eds., ASP Conf. Ser. Vol. 101, Astronomical Data Analysis Software and Systems. Astron. Soc. Pac., San Francisco, p. 17
Bolatto A. D., Wolfire M., Leroy A. K., 2013, ARA&A, 51, 207
Cormier D. et al., 2014, A&A, 564, A121
Daddi E. et al., 2015, A&A, 577, A46
Downes D., Solomon P. M., 1998, ApJ, 507, 615
Ferland G. J. et al., 2013, Rev. Mex. Astron. Astrofis., 49, 137
Gallerani S., Ferrara A., Neri R., Maiolino R., 2014, MNRAS, 445, 2848
Gruppioni C. et al., 2016, MNRAS, 458, 4297
Habing H. J., 1968, Bull. Astron. Inst. Neth., Suppl. Ser., 19, 421
Hollenbach D. J., Tielens A. G. G. M., 1999, Rev. Mod. Phys., 71, 173
Imanishi M., Nakanishi K., Izumi T., 2016, AJ, 152, 218
Kamenetzky J., Rangwala N., Glenn J., Maloney P. R., Conley A., 2016, ApJ, 829, 93
Korista K., Ferland G., Baldwin J., 1997, ApJ, 487, 555
Koss M. J. et al., 2016, ApJ, 825, 85
Lampton M., Margon B., Bowyer S., 1976, ApJ, 208, 177
Lee M.-Y. et al., 2016, A&A, 596, A85
Leitherer C. et al., 1999, ApJS, 123, 3
Lejeune T., Cuisinier F., Buser R., 1997, A&AS, 125
Levenson N. A., Weaver K. A., Heckman T. M., Awaki H., Terashima Y., 2005, ApJ, 618, 167
Lu N. Y., 1998, ApJ, 506, 673
Lu N. et al., 2017, ApJS, 230, 1
McKee C. F., Ostriker E. C., 2007, ARA&A, 45, 565
Meijerink R., Spaans M., 2005, A&A, 436, 397
Meijerink R., Spaans M., Israel F. P., 2007, A&A, 461, 793
Meijerink R. et al., 2013, ApJ, 762, L16
Murphy K. D., Yaqoob T., 2009, MNRAS, 397, 1549
Murray N., 2011, ApJ, 729, 133
Obreschkow D., Heywood I., Klöckner H.-R., Rawlings S., 2009, ApJ, 702, 1321
Panuzzo P. et al., 2010, A&A, 518, L37
Papadopoulos P. P., van der Werf P. P., Xilouris E. M., Isaak K. G., Gao Y., Mühle S., 2012, MNRAS, 426, 2601
Pereira-Santaella M. et al., 2013, ApJ, 768, 55
Pereira-Santaella M., Spinoglio L., van der Werf P. P., Piqueras López J., 2014, A&A, 566, A49
Ricci C. et al., 2017, MNRAS, 468, 1273
Risaliti G., Maiolino R., Salvati M., 1999, ApJ, 522, 157
Rosenberg M. J. F. et al., 2015, ApJ, 801, 72
Salpeter E. E., 1955, Vistas Astron., 1, 283
Schmutz W., Leitherer C., Gruenwald R., 1992, PASP, 104, 1164
Solomon P. M., Barrett J. W., 1991, in Combes F., Casoli F., eds, Proc. IAU Symp. 146, Dynamics of Galaxies and Their Molecular Cloud Distributions. Kluwer, Dordrecht, p. 235
Solomon P. M., Vanden Bout P. A., 2005, ARA&A, 43, 677
Spinoglio L., Pereira-Santaella M., Dasyra K. M., Calzoletti L., Malkan M. A., Tommasin S., Busquet G., 2015, ApJ, 799, 21
Tommasin S., Spinoglio L., Malkan M. A., Fazio G., 2010, ApJ, 709, 1257
Vallini L., Ferrara A., Pallottini A., Gallerani S., 2017, MNRAS, 467, 1300
van der Werf P. P. et al., 2010, A&A, 518, L42
Véron-Cetty M.-P., Véron P., 2006, A&A, 455, 773
Zamorani G. et al., 1981, ApJ, 245, 357
Zhao Y. et al., 2016, ApJ, 820, 118

This paper has been typeset from a TEX/LATEX file prepared by the author.